34th Annual International Conference of the IEEE EMBS
San Diego, California USA, 28 August - 1 September, 2012

# Quantitative characterization and identification of lymph nodes and nasopharingeal carcinoma by coregistered magnetic resonance images

Fabio Veronese[1], Eros Montin[2], Paolo Potepan[3], Luca T. Mainardi[2]

*Abstract*— **In this study we developed a technique to improve the identification of carcinoma and pathological lymph nodes in cases of Nasopharingeal Carcinoma (NPC), through a quantitative characterization of the tissues based on MR images: 3D VIBE (Volumetric Interpolated Breath-hold Examination) T1-CE (Contrast Enhanced), T1, T2 and Diffusion Weighted Imaging (DWI) for b-values 0,300,500,700,1000. The procedure included two phases: 1) coregistration of volumes and 2) tissue characterization.**
**Concerning the first phase, the DICOM images were reassembled spatially and resampled with isotropic 0.5mm resolution. Coregistration was performed by two multiresolution rigid transformations, merging head and neck volumes, plus a final multiresolution non rigid transformation. The anatomical 3D CE-VIBE volume was taken as reference.**
**The procedure for tissue characterization is semi automated and it required a radiologist to identify an example of tissue from the primary tumor and a metastatic lymph node. We generated a 8-dimensional membership function to perform a fuzzy-like identification of these tissues. The result of this procedure was the generation of two maps, which showed complementary characterization of lymph nodes and carcinoma. A few example will be shown to evidence the potentiality of this method in identification and characterization of NPC lesions.**

## I. INTRODUCTION

The Nasopharingeal Carcinoma (NPC) is a malignant entity that usually develops in the Rosenmueller fossa or on the roof of the nasopharynx. As with other cancers, the prognosis depends upon tumour size and infiltration of adjacent structures, lymph node involvement, and distant metastasis. To obtain NPC TNM stage evaluation PET-CT images are usually employed [1], giving informations on tissues characterized by high metabolism. In addition an MR examination is necessary to correctly identify the precise local invasion of surrounding anatomy: soft tissues, fasciae, vascular and fatty spaces [2]. Recently Diffusion Weighted MRI (DW-MRI or simply DWI) [3], has been suggested as a potential technique for NPC characterization [4][5]. High radiolabeled glucose uptake in PET identifies zones with higher metabolism, while DWI water diffusion can be related to the histology and cellular density of tissues [6]. This holds true for NPC primary tumor and metastatic lymph nodes, making of DWI a useful tool to identify such tissues [4][5]. Since experienced radiologists are able to identify pathological tissues from a MR image set, composed by 3D VIBE (Volumetric Interpolated Breath-hold Examination) T1-CE (Contrast Enhanced), T1, T2 and DWI, in this study we developed a semi-automated method for NPC pathological tissues detection and characterization based on the same set of images.

A few approaches have been already proposed to identify and segment the NPC lesion from MR images. In [7] a knowledge-based fuzzy clustering (KBF) based was employed, while in [8] a support vector machine (SVM) was used. In both the approaches, segmentation relies only on T1 weighted (T1w) images acquired pre- and post-contrast enhancement. A multi-image method (using T1w, T1w-CE and also T2w) [9] performed the segmentation through a bayesian probability estimator. In this study we consider a larger set of MR images including DWIs which are considered fundamental for the NPC characterization. We do not aim at segmenting NPC tissues, but to generate maps which quantify the similarity of each pixel with a reference structure (lymph node or carcinoma).

## II. METHODS

### A. Patient Population

The study has been carried out on 15 patients affected by NPC, 3 females and 12 males, aged between 14 and 60 at the moment of the MR examination. All of them were examined with the standard MRI protocol which implies the acquisition of these sequences:

- 3D CE-VIBE, from the skull-base to the clavicles. This is a 3D fat-sat T1 Weighted Imaging (WI) with Gadolinium contrast agent, isotropic 0.65mm resolution;TR=5.23ms,TE=2.05ms.
- T1 WI Turbo Spin Echo (TSE) for head and for neck volumes acquired separately. These sequences are 2D multi-slice axial acquisitions, with 4mm slice spacing, 0.65mm in-plane resolution; TR=572ms; TE=12ms.
- T2 WI TSE for maxillo-facial and for neck volumes acquired separately. These sequences are 2D multi-slice axial acquisitions, with 4mm slice spacing, 0.5mm in-plane resolution; TR=3180ms; TE=109ms.
- DWI series, with b-values from 0 to 1000 (0, 300, 500, 700, 1000), acquired separately for head and for neck volumes. These sequences are DW Echo-Planar Imaging (EPI) 2D multi-slice axial acquisition, with 5mm slice spacing, 2mm in-plane resolution; TR=5200ms; TE=79ms.

Except for the 3D CE-VIBE, the other sequences were acquired by axial slices and in two separate volumes, one for the head and the other for the neck.

[1]Department of Electronics and Information, Politecnico di Milano, Milan, Italy
[2]Department of Biomedical Engineering, Politecnico di Milano, Milan, Italy
[3]IRCCS Istituto Nazionale dei Tumori Foundation, Milan, Italy

978-1-4577-1787-1/12/$26.00 ©2012 IEEE

### B. Registration Method

As detailed above, the images were acquired with different spatial resolution and cover different volumes. Therefore the first task performed was the resampling of 2D slices, imposing a sampling 3D mesh aligned with the patient coordinates. The resolution chosen was 0.5mm isotropic, obtained through a linear interpolation, so that the whole image dataset had the same resolution.
These volumes were then co-registered, taking the anatomical 3D CE-VIBE volume as reference. To this purpose we used a three-step strategy:

1) multiresolution rigid registration [10] (coarse and fine correction of differences in patient position);
2) head and neck volume merging;
3) multiresolution non rigid FFD transformation [11][12] (correction of patient neck movements)

All registrations were based on Normalized Mutual Information (NMI), computed on 32 bins, and conjugated gradient descend optimization function [13]. In order to achieve the best compromise between computation time and registration detail, a hierarchical multiresolution approach has been implemented, in which the resolution of the image is increased in a coarse to fine fashion.
*Step 1* - The rigid registrations were performed on two scales. On the coarser scale registration was performed on the reference volume filtered by a gaussian kernel ($\sigma$=2.5mm), undersampled subsequently at 5mm and 2.5mm, while on the finer scale on the non smoothed 3D CE-VIBE reference, at resolution of 1mm and 0.5mm.
*Step 2* - To merge the head and neck subvolumes, the mean values of the overlapping voxels between the volumes was computed. To avoid boundary effects, voxels belonging to background (identified by a threshold) were ignored.
*Step 3* - The third step was a non rigid registration, the reference volume was filtered by a gaussian kernel($\sigma$=3mm), at resolution of 5mm and 3mm. This non rigid registration provides a description of local deformation based on a free form deformation (FFD) by employing B-splines [11][12]. The tradeoff between flexibility and computational complexity is mainly an empirical choice which is determined by the accuracy required versus the increasing in computation time. Most of the image voxels are in the background, thus to reduce calculation time we imposed a background threshold, ignoring lowest values during NMI computation.
Finally we note that DWI volumes came already aligned at different b-values thanks to their acquisition modality, thus the realignment was performed between the reference and the volume obtained with b-value=0. The resulting transform was applied to all the DWI images. The overall process is reassumed in the graph in Fig.1

### C. Tissue characterization maps

Identification and characterization of tissues, have been performed on the basis of references tissues (*templates*). Two templates were considered, the first *template* was defined with a customizable-size parallelepiped to be fully inscribed

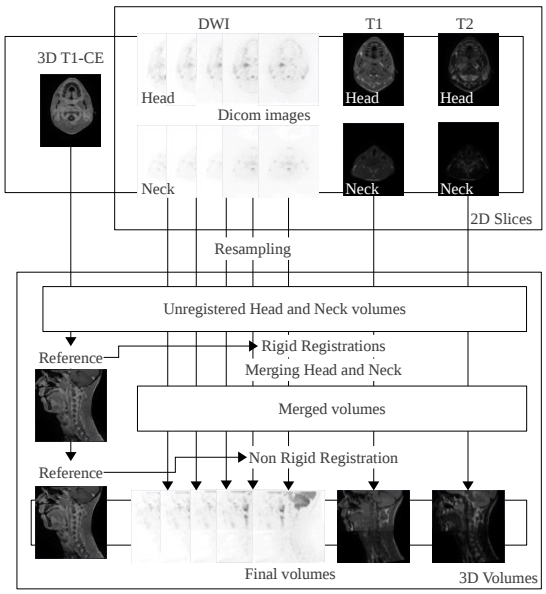


Fig. 1. Registration procedure scheme.

in the primary tumor tissue. The second *template* was defined with 9-voxel (4.5mm) sided cubes fully inscribed in the core region of pathological lymph nodes. These ROIs were used to collect data from all the 8 fused images (3D CE-VIBE, T1, T2 and 0,300,500,700,1000 b-values) and to compute histograms from each modality. These histograms (*reference histograms*) can be interpreted both as composition of *template* tissues and as probability of any other voxel to represent the tissue of the *template*. A rigorous statistic method would make use of Bayes theorem, but a 8-dimensional approach is far too complex. Thus a fuzzy-like method was developed, which uses 8 distinct membership functions. Let's $h_j^{ROI}(k)$ be the number of voxels in the $j$-th *reference histogram* whose intensity value is $k$, the membership function is defined as:

$$M_j(I_j(x,y,z)) = \frac{h_j^{ROI}(I_j(x,y,z))}{\max_k(h_j^{ROI}(k))} \tag{1}$$

where $I_j(x,y,z)$ is the intensity of voxel of coordinates $(x,y,z)$ in the image $j$. This function attributes the highest membership values to voxel whose intensity is close to the mode of $h_j^{ROI}(k)$. Correspondingly lower membership scores are given to voxel with intensity values which occur less frequently in the ROI, while 0 is given to the intensities which never occurred in the *template*. Having considered 8 different MR modalities, we computed the global membership value between the pixel (x,y,z) and the *template* as:

$$\hat{P}(x,y,z) = \sum_{j=1}^{8} M_j(I_j(x,y,z)) \cdot \frac{1000}{8} \tag{2}$$

whose resulting value is scaled between 0 and 1000. This choice attributes an higher weight to DWI modalities (which contributes to (2) with 5 out 8 elements in the sum) and it is justified by the patophysiological and diagnostical importance of the diffusion dynamic in tissues characterization.

The final map was obtained imposing a threshold value to cut the lower, less significant values:

$$P(x,y,z) = \begin{cases} \hat{P}(x,y,z) & \hat{P}(x,y,z) > th \\ 0 & otherwise \end{cases} \quad (3)$$

where $th$=250. As the tissues of interest were two, this procedure was performed twice, obtaining an identification map based on the lesion *template* while the other was based on lymph nodes *template*.

## III. RESULTS

### A. Registration

At each step of registration (before alignment, after first rigid transform, after the second rigid and after the non rigid ones) Normalized Mutual Information (NMI) and Normalized Cross Correlation (NCC) were computed to keep trace of the performance of the alignment. Both these indexes were evaluated on the image overlapping area described by a 250 voxel-sided cube located around the centre of the reference image. NMI was computed using 128 bins (versus the 32 employed in registration) histograms and cross-histogram. As it appears from the data shown (Fig.2), NMI describes a registration improvement, while NCC has a more variable trend. The largest difference is the worsening of mean NCC in steps 3 and 4 for T1 and T2 volumes. This can be explained as NMI and NCC rely on different principles: while NMI is informational based, NCC is intensity based. The similarity metrics show two major improvements related to the first rigid registration (*Step 1*) and the final not rigid registration (*Step 3*). The second rigid registration seems to be less important as its alignment is finer and involves a smaller part of the volume. The results were statistically evaluated with a t-test. The population was composed by similarity metrics computed before and after every registration step, for every image. The null hypothesis (which is expected to be refused) is that indexes at the (n+1)-th step and the n-th step follow distributions with the same mean. In Tab. I we summarize the t-test result, reporting the P-value. The test rejected always the hypothesis, except of two steps of NCC evaluation. This result can be explained by the registration multimodality. In fact NMI is based on image information content, hence its value increases with alignment, while NCC relies on the image intensity, thus it assumes negative values for aligned but counter-phase image pattern. This is a limit especially for the evaluation multimodal registrations.

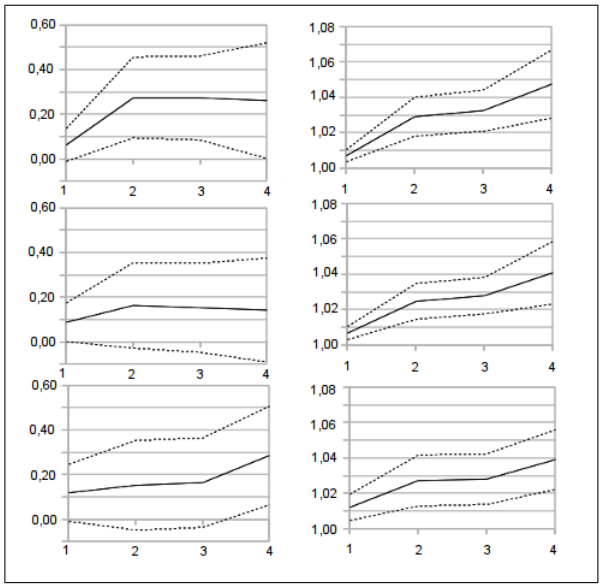


Fig. 2. Similarity metrics (mean values ± standard deviation) for raw data (1), after first rigid transform (2), second rigid transform(3), and not rigid transform (4). On the left column NCC, on the right one NMI, while from top to bottom T1, T2 and DWI statistics. These data trends show the improvement in alignment, considering that NCC performances are limited in case of multimodal image registration

TABLE I
T-TEST RESULTS AND CORRESPONDING P-VALUES.

| Reg. step P-value | | 1-2 | 2-3 | 3-4 |
|---|---|---|---|---|
| NMI | T1 | P<0.0001 | P<0.0001 | P<0.0001 |
| | T2 | P<0.0001 | P<0.0001 | P<0.0001 |
| | DWI | P<0.0001 | P<0.0001 | P<0.0001 |
| NCC | T1 | P<0.0001 | NS | P<0.0001 |
| | T2 | NS | P<0.0001 | P<0.01 |
| | DWI | P<0.0001 | P<0.0001 | P<0.0001 |

### B. Tissue identification maps

The maps obtained at the end of the processing procedure showed a behaviour depending on the target tissue. Furthermore the identified anatomical structures were complementary: the map based on primary tumor *template* detected the carcinoma itself with a good precision and retrieved also the peripheral capsule of the lymph nodes, while the lymph nodes based identification map retrieved many lymph nodes cores and detected some regions of the main carcinoma too. Hence a combined use of the maps seems to provide a detailed characterization of lymph node and NPC in the district. This can be enhanced by depicting them as coloured layers over the anatomical volume (such as in Fig.3 and Fig.4), which improves the comprehension of the surrounding anatomical features. False positives in the brain and in the spinal nerve can be easily recognized by anatomy and thus ignored.

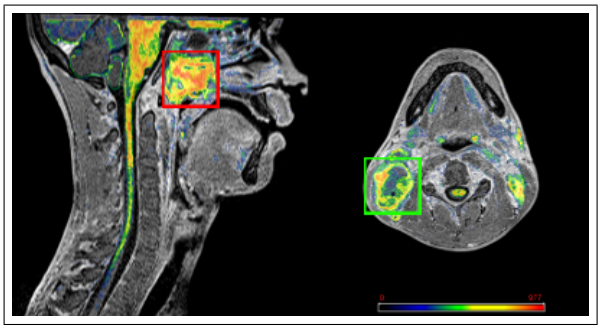

Fig. 3. Identification map rendered over the anatomical 3D CE-VIBE. This was obtained from the lesion *template*, the primary tumor is appreciated in the red box, a typical metastatic lymph node in the green one.

## IV. CONCLUSION

This study shows how a single MR examination composed with different contrast images (T1,T2,3D CE-VIBE and DWI) can collect various and different informations about the pathological tissues of NPC. The technique proposed introduces tissue characterization maps, which could be a new tool in NPC tissue identification and/or evaluation, even though these results are preliminary.

A further development will be the design of a segmentation algorithm based on the maps scores. Since the choice of the segmentation approach (threshold-based or more complex) has an high impact on the overall result, only after this improvement it will be possible to evaluate specificity and sensitivity of the overall (maps and segmentation) method.

The maps can be used as an identification tool especially where the structures of interest are tiny or their dimensions are diminished by therapy.The advantages of this technique are several: patients are not exposed to ionizing radiation, the examination is a one-step procedure, MRI costs are much lower than PET, the resolution of the resulting images is very higher.

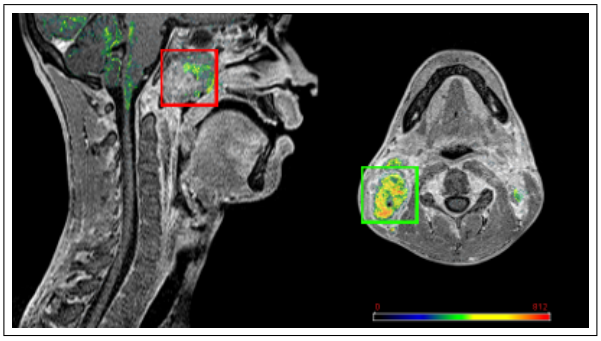

Fig. 4. Identification map rendered over the anatomical 3D CE-VIBE. This was obtained starting from the lymph nodes *template*, the primary tumor is in the red box, a metastatic lymph node in the green one.

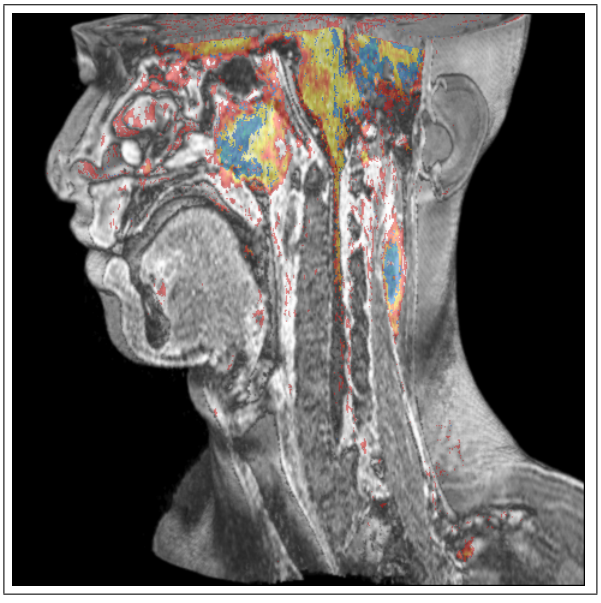

Fig. 5. 3D rendering of the anatomical 3D CE-VIBE, with a see-through cut-off region, layered with the two maps. The lesion based map is rendered in hot colors, while the lymph node based in cold.


## ACKNOWLEDGMENT

The Image Registration Toolkit was used under Licence from Ixico Ltd.


## REFERENCES


[1] Schwartz DL, Ford E, Rajendran J, et al. FDG-PET/CT imaging for preradiotherapy staging of head-and-neck squamous cell carcinoma. Int J Radiat Oncol Biol Phys. 2005;61:129-136

[2] Daisne J-F, Duprez T, Weynand B, et al. Tumor volume in pharyngo-laryngeal squamous cell carcinoma: comparison at CT, MR imaging, and FDG-PET and validation with surgical specimen. Radiology. 2004;233:93-100.

[3] Chenevert T. L., Principles of Diffusion-Weighted Imaging (DW-MRI) as Applied to Body Imaging in Diffusion-Weighted MR Imaging Springer Berlin Heidelberg 2010; 1 3-17

[4] Vandecaveye V, De Keyzer F, Vander Poorten V, et al. Head and neck squamous cell carcinoma: value of diffusion-weighted MR imaging for nodal staging. Radiology. 2009;251:131-146.

[5] Vandecaveye V, De Keyzer F, Nuyts S, et al. Detection of head and neck squamous cell carcinoma with diffusion-weighted MRI after (chemo)radiotherapy: correlation between radiologic and histopathologic findings. Int J Radiat Oncol Biol Phys. 2007;67:960-971.

[6] Patterson DM, Padhani AR, Collins DJ. Technology insight: water diffusion MRI - a potential new biomarker of response to cancer therapy. Nat Clin Pract Oncol. 2008;5:220-233.

[7] J. Zhou, T. K. Lim, V. Chong, J. Huang Segmentation and visualization of nasopharyngeal carcinoma, Comput. Biol. Med., Vol 33(5), Sept 2003, pp 407-424

[8] J. Zhou, K.L. Chan, P. Xu, V.F.H. Chong , "Nasopharyngeal carcinoma lesion segmentation from MR images by support vector machine," Biomedical Imaging: Nano to Macro, 2006. 3rd IEEE Int. Symposium, Apr 2006, pp.1364-1367

[9] F.K. Lee, D.W. Yeung, A.D. King, S.Leung, A.Ahuja, Segmentation of nasopharyngeal carcinoma (NPC) lesions in MR images, Int. J. Radiat. Oncol. Biol. Phys, Vol 61(2) Feb 2005, pp 608-620

[10] C. Studholme, D.L.G.Hill, D.J. Hawkes, An Overlap Invariant Entropy Measure of 3D Medical Image Alignment, Pattern Recognition, Vol. 32(1), Jan 1999, pp 71-86.

[11] D. Rueckert, L. I. Sonoda, C. Hayes, D. L. G. Hill, M. O. Leach, and D. J. Hawkes. Non- rigid registration using free-form deformations: Application to breast MR images. IEEE Transactions on Medical Imaging, 18(8):712-721, 1999.

[12] J. A. Schnabel, D. Rueckert, M. Quist, J. M. Blackall, A. D. Castellano Smith, T. Hartkens, G. P. Penney, W. A. Hall, H. Liu, C. L. Truwit, F. A. Gerritsen, D. L. G. Hill, and D. J. Hawkes. A generic framework for non-rigid registration based on non-uniform multi-level free-form deformations. In Fourth Int. Conf. on Medical Image Computing and Computer- Assisted Intervention (MICCAI '01), pages 573-581, Utrecht, NL, October 2001.

[13] Maes F, Collignon A, Vandermeulen D, Marchal G, Suetens P, Multimodality image registration by maximization of mutual information, IEEE Transaction on Medical Imaging. 1997; 16:187-198